Ocean Sci. Discuss., 10, 1343–1366, 2013
www.ocean-sci-discuss.net/10/1343/2013/
doi:10.5194/osd-10-1343-2013

Ocean Science
Discussions
Open Access

The instability of diffusive convection and its implication for the thermohaline staircases in the deep Arctic Ocean

S.-Q. Zhou[1], L. Qu[1,2], Y.-Z. Lu[1,2], and X.-L. Song[1,2]

[1]State Key Laboratory of Tropical Oceanography, South China Sea Institute of Oceanology, 164 West Xingang Road, Haizhu District, Guangzhou 510301, China
[2]University of Chinese Academy of Sciences, Beijing, 100049, China

Received: 28 June 2013 – Accepted: 29 July 2013 – Published: 13 August 2013

Correspondence to: S.-Q. Zhou (sqzhou@scsio.ac.cn)

Published by Copernicus Publications on behalf of the European Geosciences Union.

Abstract

In the present study, the classical description of diffusive convection is updated to interpret the instability of diffusive interfaces and the dynamical evolution of the bottom layer in the deep Arctic Ocean. In the new consideration of convective instability, both the background salinity stratification and rotation are involved. The critical Rayleigh number of diffusive convection is found to vary from 10^3 to 10^{11} in the deep Arctic Ocean as well as in other oceans and lakes. In such a wide range of conditions, the interface-induced thermal Rayleigh number is indicated to be consistent with the critical Rayleigh number of diffusive convection. In most regions, background salinity stratification is found to be the main hindrance to the occurrence of convecting layers. With the new parameterization, it is predicted that the maximum thickness of the bottom layer is 1051 m, which is close to the observed value of 929 m. And the evolution time of the bottom layer is predicted to be of the same order as that based on ^{14}C isolation age estimation.

1 Introduction

Double-diffusion is one of the most important non-mechanically driven mixing processes. It occurs in a fluid in which there are gradients of two (or more) properties with different molecular diffusivities and of opposing effects on the vertical density distribution. This phenomenon is of great interest to many disciplines in the physical sciences and engineering (Turner, 1973), but the most active research area is exploration of thermocline staircases in oceans and lakes (Schmitt, 1994; Kelley et al., 2003). Basically, there exist two modes: salt finger (SF) and diffusive convection (DC). When cold and fresh water lies on top of warm and saline water, vertical mixing is triggered by different molecular diffusion rates of heat and salt, and the DC forms (Kelley et al., 2003). The DC is characterized by a series of thermohaline staircases: a stack of homoge-

OSD
10, 1343–1366, 2013

nous mixed layers of nearly constant temperature and salinity, separated by strongly stratified thin interfaces.

As sketched in Fig. 1, each convecting layer includes a well-mixed layer and is bounded by two adjacent interfaces. In each convecting layer of DC, the fluid properties and flow dynamics can be described by four dimensionless parameters. The first one is the thermal Rayleigh number $Ra_T = \alpha g L^3 \Delta T / \nu \kappa_T$, where g is the gravitational acceleration, and α, ν, κ_T, ΔT, and L being, respectively, the thermal expansion coefficient, the kinematic viscosity, the thermal diffusivity, the temperature difference and the typical length scale of the convecting layer. The second one is the salinity Rayleigh number, $Ra_S = \beta g L^3 \Delta S / \nu \kappa_T$, where ΔS is the salinity difference and β is the haline contraction coefficient. The other two parameters are Prandtl number, $Pr = \nu / \kappa_T$, and Lewis number, $Le = \kappa_S / \kappa_T$, where κ_S is the salinity diffusivity. As the interface is the boundary of two adjacent convecting layers, the thermal Rayleigh number of the interface, Ra_{TI}, is thought to be of the same order as the critical Rayleigh number of convection, which is of the order of 1000 (Turner, 1968, 1973). This argument has been found to work well in the DC staircases in Lake Banyoles (Sánchez and Roget, 2007).

Recently, DC staircases have been observed in the deep Arctic Ocean (Timmermans et al., 2003; Timmermans and Garrett, 2006; Björk and Winsor, 2006; Carmack et al., 2012). These thermohaline staircases exhibit several unique characteristics. One of them is the thick diffusive interface. It is about 5–8 m, which is much larger than those observed in laboratory experiments (Turner, 1968; Huppert and Linden, 1979; Fernando, 1987), lakes (Sánchez and Roget, 2007; Schmid et al., 2010) and other ocean regions (Voorhis and Dorson, 1975; Larson and Gregg, 1983; Padman and Dillon, 1987; Anschutz and Blanc, 1996). In conjunction with the temperature difference across the interface, $\Delta\theta \sim 1.3 \times 10^{-3}$ °C, and other fluid properties, as listed in Table 1 below, the thermal Rayleigh number of the interface, Ra_{TI}, is of the order of 10^9, which is much larger than the typical value reported in the literature (Turner, 1968, 1973; Sánchez and Roget, 2007). Therefore, additional understanding is needed to eluci-

OSD
10, 1343–1366, 2013

date the difference between the result in the deep Arctic Ocean and those in previous studies.

Another prominent characteristic is that there exists a thick bottom mixed layer (Timmermans et al., 2003; Björk and Winsor, 2006; Timmermans and Garrett, 2006; Carmack et al., 2012). In the Canada Basin, this isothermal and isohaline bottom layer reaches to approximately 1000 m thick and extends 1000 km across the basin (Timmermans et al., 2003). Björk and Winsor (2006) proposed a simple one-dimensional diffusive-convection model to understand the dynamics of the bottom layer. However, their proposed evolution process strongly depends on turbulent eddy diffusivity, which is unavailable at the present stage, and can only explain parts of the observation. Therefore, it is necessary to seek other mechanisms that may dominate in the deep-water evolution process.

In this paper, we explore the instability of the diffusive interface using hydrographic data measured by McLane Moored Profilers (MMP) at a fixed location in the Canada Basin. The classical description proposed by Turner (1968, 1973) is extended here by considering the influences of background salinity stratification and rotation. Then the instability of the interface is discussed in comparison with the onset thermal Rayleigh number of DC. With the new parameterization, we evaluate the evolution time and thickness of the bottom layer in the deep Arctic Ocean.

2 Data

Hydrographic data were mainly obtained from the Beaufort Gyre Exploration Project (BGEP) (Ostrom et al., 2004; Proshutinsky et al., 2009). We focus on the variances of temperature and salinity in the deep ocean at a fixed location in the Beaufort Sea of Canada Basin. As marked in Fig. 2, Mooring A was deployed at 75°, 150° at the depth of 3825 m. From 2 October 2009 to 9 August 2010, the temperature and salinity between 2135 and 3080 dbar were measured by using an MMP at an interval of 8 or 11 hr. This resulted in 791 profiles. Typical potential temperature, θ, and salinity, S,

OSD
10, 1343–1366, 2013

profiles are shown in Fig. 3. In the potential temperature, θ, profile, as shown in Fig. 3a, θ decreases with increasing depth till it reaches a minimum, θ_{min}, around the depth of 2400 m. When the depth increases further, θ increases and is accompanied by obvious staircases, where the mixed layer and the interface are well resolved. Between 2950 m and the sea floor (not shown in Fig. 3), both θ and S are homogenous and uniform, this range forms the bottom layer. Similar step structures were observed in the salinity profiles (Timmermans et al., 2003; Björk and Winsor, 2006; Timmermans and Garrett, 2006). These structures are less pronounced in the salinity profiles here, as shown in Fig. 3b, due to the instruments resolution. As analyzed in our previous work (Zhou and Lu, 2013), the interface properties could be determined with an averaging technique.

In Fig. 3a, four DC steps can be identified from the potential temperature, θ, profile, which are referred to as the 1st, 2nd, 3rd and 4th steps from the bottom to the top respectively. Each step includes a mixed layer and its overlaying interface. Note that the mixed layer of the first step is the bottom layer. Usually, two parameters are used to characterize the susceptibility of water column to DC staircases. One is the density ratio R_ρ (Turner, 1965), which is expressed as

$$R_\rho = \frac{\beta \partial S/\partial z}{\alpha \partial \theta/\partial z}. \quad (1)$$

R_ρ is the ratio of the stabilizing force due to the salinity gradient and the destabilizing force due to the temperature gradient. The other one is buoyancy frequency, which has the form

$$N = [g(\alpha \partial \theta/\partial z - \beta \partial S/\partial z)]^{1/2}, \quad (2)$$

N shows the stability of the stratification of water column. It has been proposed that the shape of DC structures and the vertical heat transfer strongly depend on these parameters (see the review paper of Kelley et al., 2003). In the case of well-developed DC steps, where the mixed layer is homogeneous in temperature and salinity, $\partial S/\partial z$

OSD
10, 1343–1366, 2013

and $\partial\theta/\partial z$ are reduced to the salinity and temperature gradients across the interface. According to the definitions of Ra_T and Ra_S, R_ρ can be rewritten as $R_\rho = Ra_S/Ra_T$. For detailed analysis of the determination of the diffusive interface properties, readers are referred to Zhou and Lu (2013). The mean properties of the four interfaces are listed in Table 1.

3 The classical description of DC instability

The instability of DC has been extensively studied based on the results in laboratory experiments (Veronis, 1965; Turner, 1973; Caldwell, 1974; Huppert and Moore, 1976; Pearlstein, 1981). Basically, two modes may occur at the onset of convection; one is steady convection and the other is oscillatory convection. In the case of the ocean ($Le \sim 0.01$), it has been found that the onset Rayleigh number of steady convection appears to be less than the value for oscillatory convection (Huppert and Moore, 1976). This implies the steady convection mode is responsible for convective instability in DC staircases. In terms of linear stability analysis (Turner, 1973), the convection happens when the thermal Rayleigh number, Ra_T, exceeds a critical value, Ra_c. Ra_c is written as

$$Ra_c = \frac{Pr + Le}{Pr + 1} Ra_S + (1 + Le)\left(1 + \frac{Le}{Pr}\right)\frac{27\pi^4}{4}. \quad (3)$$

In the case of homogeneous fluid, $Ra_S = 0$ and $Le = 0$; and the equation is reduced to the onset Rayleigh number of the ordinary convection, $Ra_c = \frac{27\pi^4}{4}$.

In the deep Arctic Ocean, the DC staircases are thick and the corresponding Coriolis frequency, f, is large; one may expect that the rotation influences the occurrence of convection. The rotation is characterized by the Taylor number, $Ta = 4(\frac{fL^2}{\nu})^2$. In linear stability analysis, it has been found that the rotation inhibits the onset of convective instability (Pearlstein, 1981). When the rotation strongly affects DC, the onset Rayleigh

OSD
10, 1343–1366, 2013

number, Ra_c, would be in the form of

$$Ra_c = \frac{Pr + Le}{Pr + 1} Ra_S + (1 + Le)\left(1 + \frac{Le}{Pr}\right)\left(\frac{27\pi^4}{4}\right)^{\frac{1}{3}} Ta^{\frac{2}{3}}. \quad (4)$$

Equation (4) implies that the convection occurs when the heat-induced buoyancy force gradient overcomes the resistance produced by the salt-stratification and rotation. In the ocean, $Le \sim 0.01$ and $Pr \sim 4 - 10$; Eqs. (3) and (4) are then simplified to

$$Ra_c = \frac{Pr\, Ra_S}{Pr + 1} + \frac{27\pi^4}{4}, \quad \text{for } Ta < 10^3, \quad (5a)$$

and

$$Ra_c = \frac{Pr\, Ra_S}{Pr + 1} + \left(\frac{27\pi^4}{4}\right)^{\frac{1}{3}} Ta^{\frac{2}{3}}, \quad \text{for } Ta > 10^5. \quad (5b)$$

4 Results and discussions

Little work has been done to address the instability of DC in the ocean because the involved convective flow state is typically far beyond the onset convection regime (Carpenter, 2012). As expected from the results in previous laboratory measurements (Howard, 1964; Turner, 1968; Huppert and Linden, 1979), however, the instability mechanism of DC may actually help to understand the characteristics of diffusive interface and the bottom layer in the deep Arctic Ocean, both of which are discussed next.

4.1 Diffusive interface

In single-layer thermal convection, two thermal boundary layers exist near the top and bottom ends. Generally, it is assumed that the Rayleigh number based on the boundary

OSD
10, 1343–1366, 2013

layer thickness, Ra_δ, is of the order of the critical value, namely, $Ra_\delta \sim Ra_c$ (Howard, 1964; Siggia, 1994). This assumption has been confirmed to be marginally correct in the experiments, (Castaing et al., 1989, e.g.). In DC, as sketched in Fig. 1, each interface is the internal boundary of two adjacent convecting layers. Analogously, the same argument has been employed to study the diffusive interface instability by Turner (1968, 1973). Recently, this argument has been found to work well in the DC staircases in Lake Banyoles (Sánchez and Roget, 2007).

For the diffusive interfaces in the deep Arctic Ocean, the corresponding thermal Rayleigh number, Ra_{TI}, is obtained from its definition with the typical scale L and temperature difference ΔT being identified by the interface thickness Δh and temperature difference $\Delta\theta$. The temporal distributions of Ra_{TI} (shown in Fig. 4) indicate that Ra_{TI} of each interface is distributed approximately log-normal, which suggests that Ra_{TI} is strongly intermittent. Similar distributions have been found in vertical heat flux, eddy diffusivity and other properties (Zhou and Lu, 2013). These results imply that the deep Arctic Ocean exhibits some turbulent behaviors (Frisch, 1995). The means Ra_{TI} of all interfaces, as listed in Table 1, are of the order of $\sim 10^9$, which are much larger than the observed ($\sim 10^3$) in single-layer convection (Castaing et al., 1989) and in DC (Sánchez and Roget, 2007). One may expect that the influences of salt-stratification or rotation must be involved, that is, Eq. (5) is used to explain the results here. However, as listed in Table 1, to all interfaces, R_ρ is larger than 2 and the salinity Rayleigh number Ra_{SI} is larger than Ra_{TI}. Thus, when Ra_{SI} is employed in Eq. (5), the obtained Ra_c would be always larger than Ra_{TI}, which is in conflict with the above mentioned assumption.

In a previous laboratory study by Turner (1968), Eq. (5) was used to interpret the onset of the convecting layer in DC. When the breakdown of the unstable boundary layer is described, it has been further argued that the original salinity gradient remains unchanged because the salt diffuses much more slowly than heat. In other words, the

OSD
10, 1343–1366, 2013

salinity Rayleigh number, Ra'_S, is in the form of

$$Ra'_S = \frac{N_S^2 L^4}{\nu \kappa_T}, \tag{6}$$

where $N_S = \sqrt{g\beta \frac{\mathrm{d}S}{\mathrm{d}z}}$ is the buoyancy frequency based on the initial salinity gradient before being heated. This argument has been supported by the measurement of the advancing boundary layer in another laboratory experiment (Huppert and Linden, 1979). In the laboratory, however, the calculated Ra'_S is found to be very small due to the thin boundary layer, and it is reasonable to be negligible. Therefore, in previous studies, Ra_c is reduced to the ordinary critical Rayleigh number based on heat alone (Turner, 1968).

It is expected that the same idea can be applied to the case of interest here. As it is impossible to obtain the initial salinity gradient of the deep Arctic Ocean, the background salinity gradient is alternatively used in Eq. (6). As shown in Fig. 3b, the background salinity gradient is obtained by the linear fitting to all DC staircases in salinity profiles, resulting in $\frac{\mathrm{d}s}{\mathrm{d}z} = 1.3 \times 10^{-5}\ \mathrm{m}^{-1}$ and the corresponding $N_S = 3.1 \times 10^{-4}\ \mathrm{s}^{-1}$. Meanwhile, more data in the oceans and lakes have been collected to check the applicability of the argument. These data include the field observations in the upper layer of the Canada Basin (BGOS, 2012), deep Red Sea (Anschutz and Blanc, 1996; Swift et al., 2012), Lake Kivu (Schmid et al., 2010), Lake Banyoles (Sánchez and Roget, 2007),and the Bahamas (Larson and Gregg, 1983). Typical interface properties of these data sources are listed in Table 2.

Special attention should be paid to the comparison between the interface thermal Rayleigh number, Ra_{TI}, and the critical Rayleigh number, Ra_c. In single-layer convection, the thermal boundary layer is a small region closing to the boundary. At the boundary, the temperature gradient is the largest. Away from the boundary, the temperature gradient becomes smaller and smaller till it turns into zero in the mixed layer. This temperature distribution is result of convecting rolls (Lui and Xia, 1998). In the DC, the tem-

OSD
10, 1343–1366, 2013

perature gradient is largest inside the interface, and it gets smaller and smaller as approaching the interface end. By analogy with single-layer convection, each DC interface indeed consists of two boundary layers, as shown in Fig. 1, which are the top boundary layer of lower convecting layer and the bottom one of upper convecting layer. To the first-order approximation, the boundary layer thickness, δ, and the corresponding temperature difference, $\Delta\theta_\delta$, can be taken as $\delta \sim \Delta h/2$ and $\Delta\theta_\delta \sim \Delta\theta/2$. Consequently, the boundary layer thermal Rayleigh number, $Ra_{T\delta}$, should be $Ra_{T\delta} \sim Ra_{\mathrm{TI}}/16$. The same consideration is also applied to the salinity Rayleigh number, $Ra'_{S\delta}$, and Taylor number, Ta_δ, of the boundary layer. Typical values of these quantities are also listed in Table 2.

In terms of Eqs. (5b) and (6), the thermal critical Rayleigh number, Ra_c, is obtained from the δ-based salinity Rayleigh number, $Ra'_{S\delta}$, and the δ-based Taylor number, Ta_δ. Note that Eq. (5a) is used when $Ta < 1000$. Within the collected data, the thermal critical Rayleigh number, Ra_c is found to vary in a wider range from 10^3 in the Lake Banyoles to 10^{11} in the deep red Sea, which are shown in Fig. 5a. Figure 5a also exhibits that the calculated thermal critical Rayleigh number, Ra_c, is very close to the δ-based thermal Rayleigh number, $Ra_{T\delta}$, in almost all the collected data. As some data were captured from the published figures (Sánchez and Roget, 2007; Larson and Gregg, 1983), the limited accuracy would be the most probable reason responsible for the data scatters in Fig. 5a. To the well statistical data, e.g. those in the upper Arctic (BGOS, 2012), Ra_c is in good agreement with $Ra_{T\delta}$. As far as we know, this is the first time that the classical description of DC has been applied to interpret instability of diffusive interfaces in the ocean.

In addition, we examine the influences of background salinity stratification and the rotation on the onset of convection. The comparison between the first and the second terms in Eq. (5b) is plotted in Fig. 5b. In the deep Arctic Ocean, the influence of rotation is supposed to be the largest because of the thickest diffusive interface and the largest Coriolis frequency in all the data. Even so, the contribution of rotation is found to be about 1000 times smaller than that of the salinity stratification. In other regions, the con-

OSD
10, 1343–1366, 2013

tribution of rotation is even smaller. Therefore, background salinity stratification would be the main hindrance to the occurrence of convective flow in the ocean. The influence of the salinity stratification, however, is not always important. In the Lake Banyoles, as shown in Fig. 5b, it is found that $Ra'_{S\delta} \sim 50$; thus, the inherent mechanism of thermal convection plays a dominating role there, $Ra_{T\delta} \sim 1000$ in Sánchez and Roget (2007).

4.2 Bottom homogenous layer

As introduced in Sect. 1, the thick homogenous bottom layer is an unique feature of the deep Arctic Ocean (Timmermans et al., 2003; Björk and Winsor, 2006; Timmermans and Garrett, 2006; Carmack et al., 2012; Zhou and Lu, 2013). As the model proposed by Björk and Winsor (2006) cannot well explain the dynamics of the bottom layer, we attempt to find other mechanisms. Recently, more evidence has been collected that geothermal heating plays an important role in the hydrographic configuration of deep water in the Arctic Ocean (Timmermans et al., 2003; Björk and Winsor, 2006; Timmermans and Garrett, 2006; Carmack et al., 2012; Zhou and Lu, 2013). The situation that the weakly-stratified deep Arctic Ocean is being heated by geothermal heating is similar to those studied in the laboratory experiments and numerical simulations, where DC occurred in salt-stratified fluid heated from below (Turner, 1968; Huppert and Linden, 1979; Fernando, 1987). Thus, it is interesting to examine whether the results obtained from the laboratory experiments can be applied to the deep ocean and whether it can shed more light on the deep water dynamic process.

In the laboratory experiments where salt-stratified fluid was heated from below (Turner, 1968, 1973; Huppert and Linden, 1979; Fernando, 1987), it has also been found that the bottom layer is much thicker than the overlaying staircases, which is similar to the finding in the deep Arctic Ocean. In Turner's (1968) theoretical work, he suggested that the homogeneous bottom layer reaches a critical thickness before a second convecting layer appears on top of it. When the instability of DC follows the

OSD
10, 1343–1366, 2013

above arguments based on Eqs. (5) and (6), this maximum thickness is deduced as,

$$h_{c1} = \left(\frac{\frac{1}{4} Ra_c \nu {q_0}^3}{\kappa^2 N_S^8} \right)^{\frac{1}{4}}, \quad (7)$$

here q_0 is the buoyancy flux, which is derived as $q_0 = \alpha g F / \rho_0 c_p$, and F is the heat flux supplied from the bottom boundary. Eq. (7) has been verified in Turner's laboratory except that the fitted Ra_c was about $\sim 2.4 \times 10^4$, which is much larger than the ordinary value of ~ 1000. Coincidentally, as discussed in last subsection, the fitted Ra_c is very close to the interface thermal Rayleigh number, Ra_{TI}. In the deep Arctic Ocean, geothermal heating is taken as $F \sim 50\,\mathrm{mW\,m^{-2}}$ (Langseth et al., 1990). At Mooring A, the physical properties of sea water are respectively $\alpha = 1.27 \times 10^{-4}\,^{\circ}\mathrm{C}^{-1}$, $\beta = 7.5 \times 10^{-4}$, $\nu = 1.85 \times 10^{-6}\,\mathrm{m^2\,s^{-1}}$, $\kappa = 1.39 \times 10^{-7}\,\mathrm{m^2\,s^{-1}}$, $g = 9.8\,\mathrm{m\,s^{-2}}$, $\rho_o = 1041.3\,\mathrm{kg\,m^{-3}}$, and $c_p = 3899.1\,\mathrm{J\,kg^{-1}\,^{\circ}C}$. With the related properties of the first interface, as listed in Table 1, h_{c1} is calculated to be 526 m, which is smaller than the observed value of 929 m (Zhou and Lu, 2013). However, as proposed by the laboratory work, if Ra_c is replaced by Ra_{TI} in Eq. (7), h_{c1} is found to be 1051 m, which is much closer to the observed value.

In another laboratory study, Fernando (1987) found that the bottom mixed layer still grows upwardly even after the second mixed layer forms. Based on the assumption that the kinetic and potential energies of turbulent eddies are balanced when the mixed layer grows to a critical height, an alternative expression for the layer thickness has been proposed,

$$h_{c2} = 41.5 \left(\frac{q_0}{N_S^3} \right)^{\frac{1}{2}}. \quad (8)$$

With the properties of the interface, the thickness h_{c2} is found to be 29 m, which is much smaller than the observation. Therefore, the assumption of energy balance cannot explain the formation of the bottom layer.

OSD
10, 1343–1366, 2013

In a study of ^{14}C isolation age, the deep water of the Canada Basin is estimated to be about 500 yr old (Macdonald et al., 1993). According to the laboratory study of Turner (1968), the evolution time of the bottom layer can be predicted by

$$\tau = \frac{(N_S h)^2}{2q_0} \tag{9}$$

before the formation of the secondary convecting layers. Supposing that the bottom layer thickness, h, is about 1000 m, the time τ is calculated to be $\tau = 109$ yr. In observations, however, there are more than four thermohaline staircases overlying the bottom layer, which means that the evolution time of the bottom layer must be longer than τ. In some sense, τ can be regarded as the lower bound of evolution time of the bottom layer.

Based on the above results, it is suggested that the homogenous bottom layer is the result of geothermal heating under salinity stratification. Its maximum thickness can be described by Eq. (7), where Ra_{TI} is alternatively used. This implies that the evolution of bottom layer is mainly controlled by the convective instability mechanism. The time, τ, is inferred to be of the same order as that estimated from the ^{14}C isolation age detection, which also suggests that the main evolution mechanism of the deep water in deep Arctic Ocean is similar to that in the laboratory experiments (Turner, 1968, 1973; Huppert and Linden, 1979; Fernando, 1987).

5 Conclusions

In summary, the classical description of DC has been updated to interpret the instability of diffusive interfaces and the dynamical characteristics of the bottom layer in the deep Arctic Ocean. When both background salinity stratification and rotation are considered, the critical Rayleigh number, Ra_c, of DC is found to vary in a wide range from 10^3 to 10^{11} within the collected data. And the thermal Rayleigh number of boundary layers,

OSD
10, 1343–1366, 2013

$Ra_{T\delta}$, is consistent with the critical Rayleigh number, Ra_c, of DC. It is expected that this new parameterization of Eqs. (5) and (6) can be extensively applied to DC in other oceans and lakes. In most cases, the salinity stratification is found to be the main hindrance to the occurrence of convective flow except for regions where the diffusive interface is thin, e.g., in Lake Banyoles. When the interface thermal Rayleigh number, $Ra_{T|}$, is alternatively employed in the old parameterization of Eq. (7), the predicted maximum thickness of the bottom layer is 1051 m, which is close to the observed value of 929 m. The evolution time of the bottom layer, τ, is predicted to be ~ 100 yr, which is of the same order as the ^{14}C isolation age estimate. As multi-layers overlaying the bottom layer, the evolution time of of water in the deep Arctic Ocean must be longer than τ, and τ can be taken as the lower bound of the resident time.

In the formation of deep Arctic water, one perhaps cannot exclude the effects of other instabilities, e.g. thermobaric convection (Carmack et al., 2012) or topographic Rossby waves formed as a result of instability of a strong current (Timmermans et al., 2010). Nonetheless, according to the results in this study, the main evolution mechanism of the deep water would be similar to that in the laboratory experiments where salt-stratified fluid was heated from below (Turner, 1968, 1973; Huppert and Linden, 1979; Fernando, 1987). Therefore, when the classical description of DC is updated, it can be applied to interpret the main flow dynamics of the deep Arctic Ocean.

Acknowledgements. We thank Mary-Louise Timmermans and Martin Schmid for their constructive comments. This work was supported by China NSF grants (41176027 and 11072253), Guangdong NSF (10251030101000000), and the 973 Program (2010CB950302). The data were collected and made available by the Beaufort Gyre Exploration Program based at the Woods Hole Oceanographic Institution (http://www.whoi.edu/beaufortgyre) in collaboration with researchers from Fisheries and Oceans Canada at the Institute of Ocean Sciences.

OSD
10, 1343–1366, 2013

References

Anschutz, P. and Blanc, G.: Heat and salt fluxes in the Atlantis II Deep (Red Sea)., Earth Planet. Sc. Lett, 142, 147–159, doi:10.1016/0012-821X(96)00098-2, 1996. 1345, 1351, 1361

BGOS: The hydrographic data measured by the Ice-Tethered Profiler 2 (ITP2) in Beaufort Gyre Observing System (BGOS) were used in the present work., available at: http://www.whoi.edu/itp, last access: 10 August 2012. 1351, 1352

Björk, G., and Winsor, P.: The deep waters of the Eurasian Basin, Arctic Ocean: geothermal heat flow, mixing and renewal, Deep Sea Res. Pt. I, 53, 1253–1271, doi:10.1016/j.dsr.2006.05.006, 2006. 1345, 1346, 1347, 1353

Caldwell, D. R.: Experimental studies on the onset of thermohaline convection, J. Fluid Mech., 64, 347–368, doi:10.1017/S0022112074002436, 1974. 1348

Carmack, E. C., Williams, W. J., Zimmermann, S. L., and McLaughlin, F. A.: The Arctic Ocean warms from below, J. Geophys. Res., 39, L07604, doi:10.1029/2012GL050890, 2012. 1345, 1346, 1353, 1356

Carpenter, J. R., Sommer, T., and Wuest, A.: Stability of a double-diffusive interface in the diffusive convection regime, J. Phys. Oceanogr., 42, 840–854, doi:10.1175/JPO-D-11-0118.1, 2012. 1349

Castaing, B., Gunaratne, G., Heslot, F., Kadanoff, L., Libchaber, A., Thomae, S., Wu, X.-Z., Zaleski, S., and Zanetti, G.: Scaling of hard thermal turbulence in Rayleigh–Bénard convection, J. Fluid.Mech., 204, 1, doi:10.1017/S0022112089001643, 1989. 1350

Fernando, H. J. S.: The formation of layered structure when a stable salinity gradient is heated from below, J. Fluid. Mech., 182, 525–541, doi:10.1017/S0022112087002441, 1987. 1345, 1353, 1354, 1355, 1356

Frisch, U.: Turbulence: the Legacy of A. N. Kolmogorov, Cambridge University Press, UK, 1995. 1350

Howard, L. N.: Convection at high Rayleigh number, edited by: Grtler, H., Proc. 11th Cong. Applied Mech., 1964. 1349, 1350

Huppert, H. E. and Linden, P. F.: On heating a stable salinity gradient from below, J. Fluid. Mech., 95, 431–464, doi:10.1017/S0022112079001543, 1979. 1345, 1349, 1351, 1353, 1355, 1356

Huppert, H. E. and Moore, D. R.: Nonlinear double-diffusive convection, J. Fluid. Mech., 78, 821–854, doi:10.1017/S0022112076002759, 1976. 1348

OSD
10, 1343–1366, 2013

Kelley, D. E., Fernando, H. J. S., Gargett, A. E., Tanny, J., and Özsoy, E.: The diffusive regime of double diffusive convection, Prog. Oceanogr., 56, 461–481, doi:10.1016/S0079-6611(03)00026-0, 2003. 1344, 1347

Langseth, M. G., Lachenbruch, A., and V.Marshall, B.: Geothermal Observations in the Arctic Region, The Geology of North America: the Arctic Ocean Region, The Geological Society of America, 1990. 1354

Larson, N. G. and Gregg, M. C.: Turbulent dissipation and shear in thennohaline intrusions, Nature, 306, 26–32, doi:10.1038/306026a0, 1983. 1345, 1351, 1352, 1361

Lui, S. L. and Xia, K. Q.: Spatial structure of the thermal boundary layer in turbulent convection, Phys. Rev. E, 57, 5494–5503, doi:10.1103/PhysRevE.57.5494, 1998. 1351

Macdonald, R., Carmack, E. C., and Wallace, D. W. R.: Tritium and radiocarbon dating of Canada basin deep waters, Science, 259, 103–104, doi:10.1126/science.259.5091.103, 1993. 1355

Ostrom, W., Kemp, J., Krishfield, R., and Proshutinsky, A.: Beaufort Gyre freshwater experiment: deployment operations and technology in 2003, Technical Report WHOI-2004-1, Woods Hole Oceanographic Institution, 2004. 1346

Padman, L. and Dillon, T. M.: Vertical heat fluxes through the Beaufort Sea thermohaline staircase, J. Geophys. Res., 92, 10799–10806, doi:10.1029/JC092iC10p10799, 1987. 1345

Pearlstein, A. J.: Effect of rotation on the stability of a doubly diffusive fluid layer, J. Fluid Mech., 103, 3389–412, doi:10.1017/S0022112081001390, 1981. 1348

Proshutinsky, A., Krishfield, R., Timmermans, M.-L., Toole, J., Carmack, E., McLaughlin, F., Williams, W. J., Zimmermann, S., Itoh, M., and Shimada, K.: Beaufort Gyre freshwater reservoir: state and variability from observations, J. Geophys. Res., 114, C00A10, doi:10.1029/2008JC005104, 2009. 1346

Sánchez, X., and Roget, E.: Microstructure measurements and heat flux calculations of a triple-diffusive process in a lake within the diffusive layer convection regime, J. Geophys. Res., 112, C02012, doi:10.1029/2006JC003750, 2007. 1345, 1350, 1351, 1352, 1353, 1361

Schmid, M., Busbridge, M., and Wüest, A.: Double diffusive convection in Lake Kivu, Limnol. Oceanogr., 55, 225–238, doi:10.4319/lo.2010.55.1.0225, 2010. 1345, 1351, 1361

Schmitt, R. W.: Double diffusion in oceanography, Annu. Rev. Fluid Mech., 26, 255–285, doi:10.1146/annurev.fl.26.010194.001351, 1994. 1344

Siggia, E. B.: High Rayleigh number convection, Annu. Rev. Fluid Mech., 26, 137–168, doi:10.1146/annurev.fl.26.010194.001033, 1994. 1350

OSD
10, 1343–1366, 2013

Swift, S. A., Bower, A. S., and Schmitt, R. W.: Vertical, horizontal, and temporal changes in temperature in the Atlantis II and discovery hot brine pools, Red Sea, Deep Sea Res. I, 64, 118–128, doi:10.1016/j.dsr.2012.02.006, 2012. 1351, 1361

Timmermans, M. L. and Garrett, C.: Evolution of the deep water in the Canadian Basin of the Arctic Ocean, J. Phys. Oceanogr., 36, 866–874, doi:10.1175/JPO2906.1, 2006. 1345, 1346, 1347, 1353

Timmermans, M. L., Garrett, C., and Carmack, E.: The thermohaline structure and evolution of the deep waters in the Canada Basin, Arctic Ocean, Deep Sea Res. Pt. I, 50, 1305–1321, doi:10.1016/S0967-0637(03)00125-0, 2003. 1345, 1346, 1347, 1353

Timmermans, M. L., Rainville, L., Thomas, L., and Proshutinsky, A.: Moored observations of bottom-intensified motions in the deep Canada Basin, Arctic Ocean, J. Mar. Res., 68, 625–641, doi:10.1357/002224010794657137, 2010. 1356

Turner, J. S.: The coupled turbulent transport of salt and heat across a sharp density interface, Int. J. Heat. Mass. Tran., 8, 759–767, doi:10.1016/0017-9310(65)90022-0, 1965. 1347

Turner, J. S.: The behavior of a stable salinity gradient heated from below, J. Fluid. Mech., 33, 183–200, doi:10.1017/S0022112068002442, 1968. 1345, 1346, 1349, 1350, 1351, 1353, 1355, 1356

Turner, J. S.: Buoyancy Effects in Fluids, Cambridge University Press, 1973. 1344, 1345, 1346, 1348, 1350, 1353, 1355, 1356

Veronis, G.: On finite amplitude instability in thermohaline convection, J. Mar. Res., 23, 1–17, 1965. 1348

Voorhis, A. D. and Dorson, D. L.: Thermal convection in the Atlantis II hot brine pool, Deep Sea Res., 22, 167–175, doi:10.1016/0011-7471(75)90056-X, 1975. 1345

Zhou, S.-Q., and Lu, Y.-Z.: Characterizations of double diffusive convection steps and heat budget in the deep Arctic Ocean, J. Geophys. Res., in revision, 2013. 1347, 1348, 1350, 1353, 1354

OSD
10, 1343–1366, 2013

Table 1. Mean properties of four diffusive interfaces at Mooring A between 2 October 2009 and 9 August 2010. They are potential temperature difference, $\Delta\theta$, salinity difference, ΔS, and thickness, Δh, density ratio, R_ρ, buoyancy frequency, N, thermal Rayleigh number, Ra_{TI}, salinity Rayleigh number, Ra_{SI}, and Taylor number, Ta_{I}.

Interface	1	2	3	4
$\Delta\theta$ (10^{-3} °C)	1.79	1.25	1.34	0.96
ΔS (10^{-4})	6.46	5.11	8.23	5.26
Δh (m)	7.79	6.29	8.61	5.32
R_ρ	2.13	2.46	3.67	3.27
N (10^{-4} s^{-1})	5.86	6.14	7.36	7.46
Ra_{TI} (10^9)	3.91	1.43	4.11	0.59
Ra_{SI} (10^9)	8.33	3.52	15.1	1.96
Ta_{I} (10^7)	2.13	0.91	3.18	0.46

OSD
10, 1343–1366, 2013

Table 2. Data used in the analysis. The average values are listed when more than one dataset are included in the data source. There are temperature difference, $\Delta\theta$, salinity difference, ΔS, thickness, Δh, and Prandtl number, Pr, of the interface; saline buoyancy frequency, N_S, based on the background salinity profile; Taylor number, Ta_δ, thermal Rayleigh number, $Ra_{T\delta}$, and salinity Rayleigh number, $Ra'_{S\delta}$ of the boundary layer. Deep Arctic – data of the present work; Upper Arctic – Average data measured by the ice-tethered profiler (ITP) 2 in the Beaufort Gyre Observation system (BGOS); Atlantis II 1 – Fig. 4 of Anschutz and Blanc (1996); and Atlantis II 2 – Fig. 4 of Swift et al. (2012); Lake Kivu – Fig. 1 and Table 2 of Schmid et al. (2010); Lake Banyoles – Figs. 2 and 8 of Sánchez and Roget (2007); and the Bahamas – Fig. 2 of Larson and Gregg (1983).

Location	$\Delta\theta$ ($^\circ C$)	ΔS	Δh (m)	Pr	N_S (s^{-1})	$Ra_{T\delta}$	$Ra'_{S\delta}$	Ta_δ
Deep Arctic	0.0012	0.00063	6.74	13.3	0.00031	1.3×10^8	6.2×10^7	9.5×10^5
Upper Arctic	0.044	0.016	0.62	13.3	0.0056	1.7×10^6	1.3×10^6	62.0
Atlantis II 1	4.082	30.08	1.70	3.8	0.14	6.3×10^{10}	9.4×10^{10}	3.7×10^3
Atlantis II 2	4.436	30.09	1.92	4.3	0.17	1.2×10^{11}	2.9×10^{11}	6.6×10^3
Lake Banyoles	0.360	0.073	0.018	6.2	–	1.7×10^3	55.1	8.9×10^{-5}
Lake Kivu	0.0045	–	0.19	6.2	0.0086	3.5×10^4	4.3×10^4	2.5×10^{-3}
Bahamas	0.047	0.026	0.069	6.4	0.018	2.2×10^4	3.8×10^3	6.8×10^{-3}

OSD
10, 1343–1366, 2013

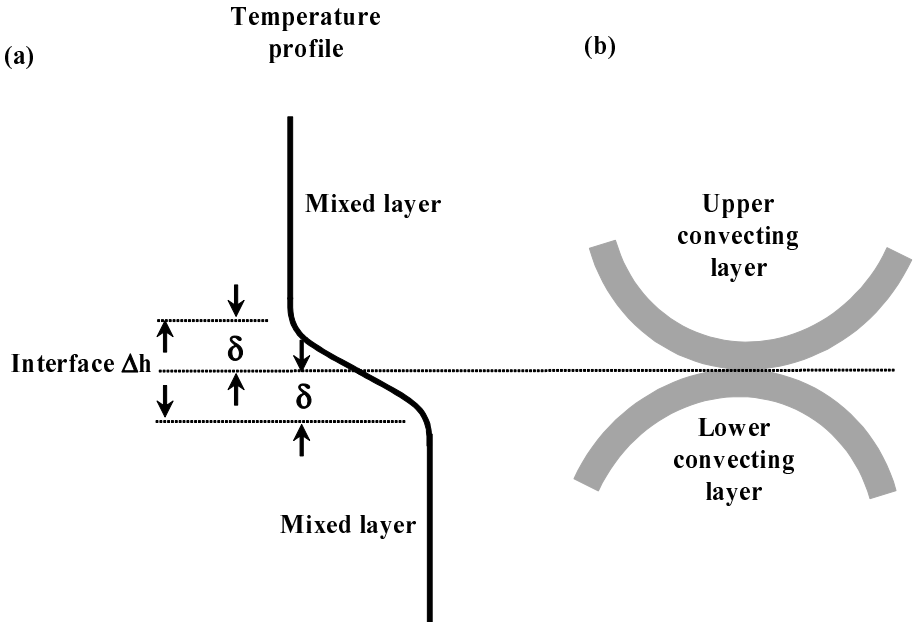

Fig. 1. (a) A sketch of temperature distribution of a diffusive interface in DC staircases; **(b)** a cartoon of flow pattern near the interface.

OSD
10, 1343–1366, 2013

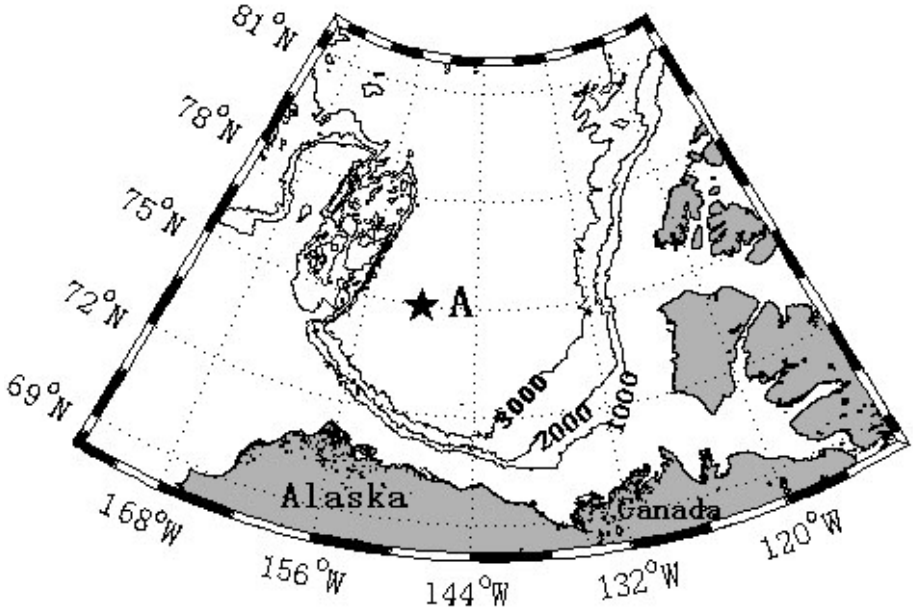

Fig. 2. Map of the Canada Basin in the Arctic Ocean. Isobaths are plotted using the ETOP data. The location of Mooring A is marked by a star.

OSD
10, 1343–1366, 2013

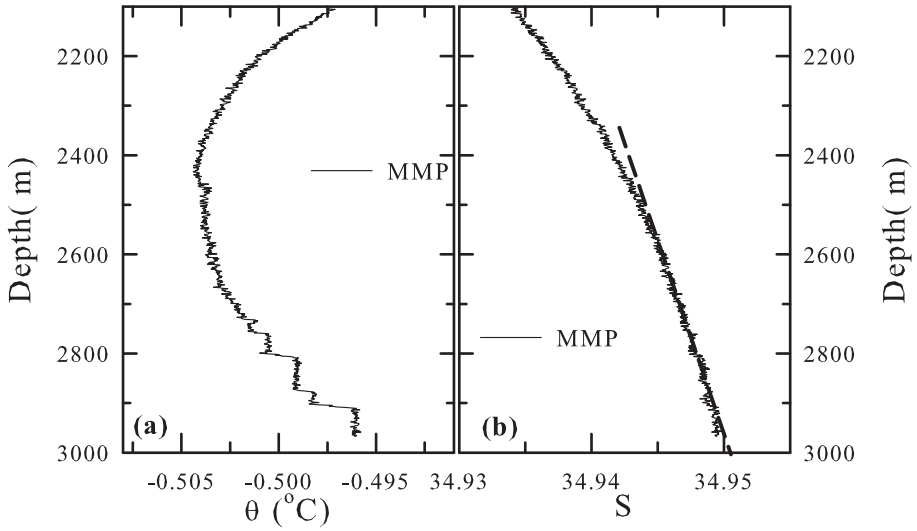

Fig. 3. Profiles of **(a)** potential temperature (θ) and **(b)** salinity (S) at Mooring A on 7 August 2010. The dashed line is the linear fit of the DC staircases in the salinity profile.

OSD
10, 1343–1366, 2013

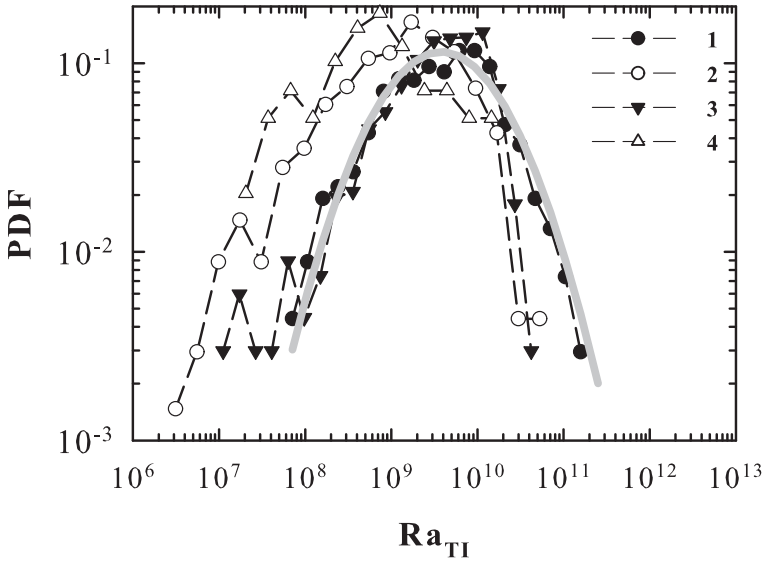

Fig. 4. Probability density functions (PDFs) of thermal Rayleigh number, Ra_{TI}, of the four diffusive interfaces. Data of the first, second, third and fourth interfaces are plotted using the dashed lines with solid circles, open circles, solid down triangles and open triangles, respectively. The lognormal fitting of PDF of the first interface is shown as a gray curve.

OSD
10, 1343–1366, 2013

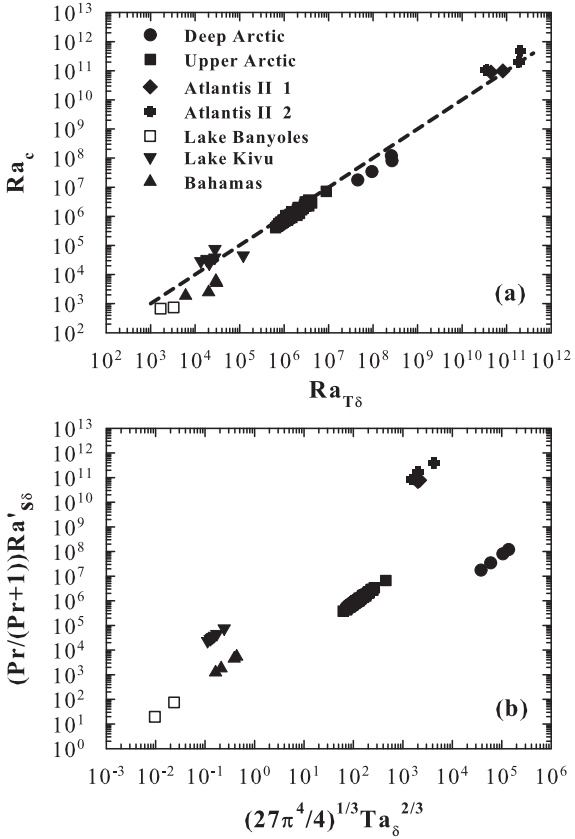

Fig. 5. (a) Comparison between the calculated onset thermal Rayleigh number, Ra_c, based on Eq. (5) and the boundary layer thermal Rayleigh number, $Ra_{T\delta}$. **(b)** Comparison between the first term, $Pr\,Ra'_{S\delta}/(Pr+1)$, and the second term, $(27\pi^4/4)^{1/3}Ta_\delta^{2/3}$, in Eq. (5b).

OSD
10, 1343–1366, 2013